Journal of The Electrochemical Society, **150** (6) E293-E298 (2003)
0013-4651/2003/150(6)/E293/6/$7.00 © The Electrochemical Society, Inc.

Mott-Schottky Analysis of Nanoporous Semiconductor Electrodes in Dielectric State Deposited on $SnO_2(F)$ Conducting Substrates

Francisco Fabregat-Santiago,[a] Germà Garcia-Belmonte,[a] Juan Bisquert,[a,*,z] Peter Bogdanoff,[b] and Arie Zaban[c,*]

[a]*Department de Ciències Experimentals, Universitat Jaume 1, 12080 Castelló, Spain*
[b]*Department Solare Energetik, Hahn-Meitner Institut, 14109 Berlin, Germany*
[c]*Department of Chemistry, Bar-Ilan University, Ramat-Gan 52900, Israel*

This paper analyzes the dark capacitance of nanostructured electrodes in the dielectric state, with particular emphasis on TiO_2 electrodes deposited over a transparent conducting substrate of $SnO_2(F)$. It is shown that at those potentials where the TiO_2 nanostructure is in the dielectric state, the capacitance is controlled by the contact $SnO_2(F)$/(electrolyte, TiO_2). The partial or total covering of the substrate by a dielectric medium causes a modification of the Mott-Schottky plot of the bare substrate. We provide a mapping of the various Mott-Schottky curves that will appear depending on the film characteristics. If the dielectric nanoparticles completely block part of the substrate surface, the slope of the Mott-Schottky plot increases (with the same apparent flatband potential) as an effect of area reduction. The covering of a significant fraction of the surface by a thin dielectric layer shifts the apparent flatband negatively. Measurements on several TiO_2 nanostructured electrodes show that the capacitance contribution of the semiconductor network in the dielectric state is very low, indicating that the field lines penetrate little into the TiO_2 network, not much further than the first particle. The different surface covering observed for rutile-anatase and pure anatase colloids is explained by lattice matching rules with the substrate. By comparing different electrodes, the Helmholtz capacitance at the $SnO_2(F)$/solution interface was calculated and the apparent flatband potential was corrected for the effect of band unpinning.
 [DOI: 10.1149/1.1568741]

Manuscript submitted May 1, 2002; revised manuscript received December 8, 2003. Available electronically April 10, 2003.

Nanoscaled materials have become very important for recent technological developments in broad fields such as photovoltaics, photocatalysis, energy storage (batteries, supercapacitors), electrochromic devices, etc. Nanostructured electrode materials may belong, for example, to the groups of porous semiconductors, organic nanocomposites, or sintered nanoporous metal oxides. In particular, nanostructured semiconductor electrodes, and especially nanoporous TiO_2, have raised widespread attention for their use in several photoelectrochemical applications such as dye-sensitized nanocrystalline solar cells (DSSCs).[1] This kind of electrodes consists of nanoparticulate semiconductor networks composed of small and low-doped metal-oxide crystallites (in the 10 nm range), sintered in a connected structure on top of a conducting substrate. These systems involve three different phases: the transparent conducting substrate of F-doped SnO_2, the porous TiO_2 network, and the electrolyte. Because of the small size of the nanoparticles and the intricate geometry of the porous network permeated with electrolyte, new methods and models are required to describe these systems.

When a nanoporous electrode reaches equilibrium in the dark,[2] the three phases involved, having different work functions, equilibrate at a unique value of the Fermi level and redox potential. Because in equilibrium most of the semiconductor nanostructure is inert electrically, charge separation and electrical fields are confined to the contact between the substrate and the electrolyte, and also to the nanoparticles closest to the substrate.[2] This contact $SnO_2(F)$/(electrolyte, TiO_2) has been discussed in several works.[2-12]

Here we analyze the information that can be obtained on the $SnO_2(F)$/(electrolyte, TiO_2) contact properties from capacitance measurements applying Mott-Schottky (MS) analysis. We consider the capacitance-voltage relationship of the conducting $SnO_2(F)$ substrate partially or totally covered by a dielectric medium. The objective is to compare the capacitance of the nanoporous electrode to that of the bare substrate in order to characterize the properties of the former.

With respect to DSSCs, there are several points of interest to this study. It is useful to determine the exposed substrate area in a reliable way, because charge transfer from the substrate could cause a significant loss of photogenerated electrons.[12] It is also interesting to evaluate the influence of charge stored in the capacitor at the $SnO_2(F)$/(electrolyte, TiO_2) contact in electrochemical measurement techniques.[13,14] An alternative way to obtain the information supplied by capacitance measurements is to monitor the electrical fields in the substrate by interference reflection measurements,[11] so it is important to develop comparison tools for future work. Finally, a possible influence of the dark potential drop in the nanoparticles[6] on the photovoltage obtained in DSSC should be explored. An analogy with the *p-n* junction mechanism has been suggested,[6] but the issue is still controversial.[7,9,10]

Although nanoporous TiO_2 on conducting SnO_2 substrate is taken here as the specific example of reference, the aim of this research is more general. So far, a wide variety of types of nanoporous electrodes has been reported in the literature concerning methods of preparation, materials and mixtures, size and doping of nanoparticles, surface covering treatments, etc., and the field will presumably grow in the future. Accordingly, we provide in this report a mapping of the various MS curves that will appear depending on the film characteristics. This will enable good characterization of the electrode, not only as prepared, but also following the possible changes during the electrochemical manipulations, by such effects as intercalation, change of contact area, change of doping, etc.

Background

The substrate capacitance.—In the nanoporous electrodes the electrolyte permeates the semiconductor network voids up to the substrate. Therefore the conducting substrate of fluor-doped tin oxide ($SnO_2(F)$) is in contact with the electrolyte (electrical pathway i in Fig. 1). At stationary potentials that are positive with respect to the flatband potential, highly doped semiconductor films develop a space-charge region at the surface, which provides a capacitance per area unit C_b (band bending). The capacitance C_b is about the same order of the Helmholtz capacitance C_H; thus, the situation is an intermediate to the limits of band-edge pinning and Fermi level pinning. The effect of the band unpinning can be treated[15] as summarized in the Appendix. According to Eq. A-10, a linear MS plot is predicted, and this is observed as reported in Ref. 16-18. The effect of the variation of Helmholtz potential is to shift the observed

* Electrochemical Society Active Member.
z E-mail: bisquert@uji.es

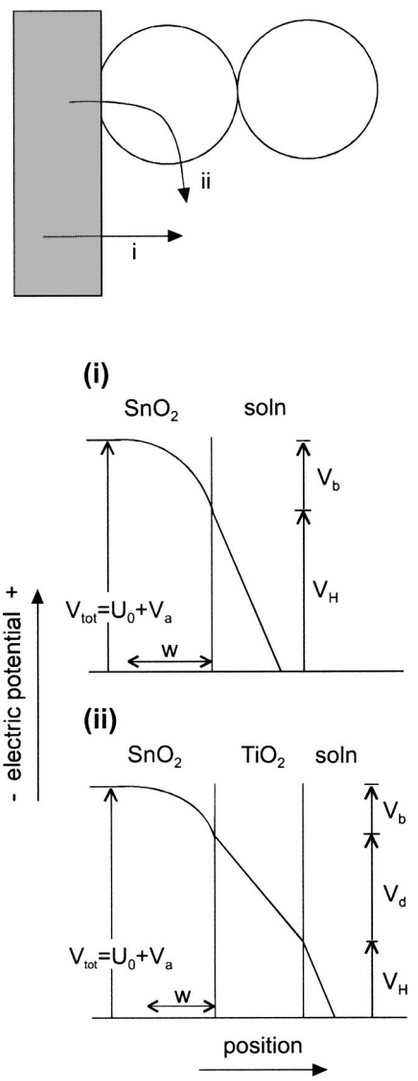

Figure 1. Scheme of the three-phase contact between the substrate conducting SnO_2 film, the porous TiO_2 network, and the electrolyte. The lower diagrams show the electrical potential distribution in pathway i (SnO_2/solution) and ii (SnO_2 /TiO_2/solution). Note that this representation is inverted with respect to band bending (electron energy).

MS plot negatively, so that: (*i*) the slope of C^{-2} *vs. V* does not change with respect to that predicted in band-edge pinning conditions, $2/(N_D e \varepsilon_r \varepsilon_0)$, and (*ii*) the apparent flatband potential is $-(U_0 + U_1)$, which is shifted negatively from the real flatband potential $(-U_0)$ by an amount[15,18]

$$U_1 = \frac{N_D e \varepsilon_r \varepsilon_0}{2C_H^2} \quad [1]$$

Electronic properties of the porous semiconductor network.—The TiO_2 used in nanostructured photoelectrodes is usually very lightly doped, and in equilibrium in the dark it contains a negligible number of free electrons. Thus, it can be considered that TiO_2 matrix contains no space charge of any kind, and it behaves as a dielectric.[2,4]

When the TiO_2 is in the dielectric state the electrical field inside the particles is governed by the Laplace equation. Because of the small size of the nanoparticles surrounded with electrolyte, it is impossible to sustain large-scale electrical fields in the semiconductor network. The theoretical analysis[2] indicates that the electrical field at the SnO_2(F)/TiO_2 junction penetrates the porous network to a small distance, in the order of a few particles. Several reports[4,6,10] are in agreement with this result.

The TiO_2 phase can be taken to electron accumulation state, either by negative potential bias or by photogeneration. Obviously in that state the TiO_2 cannot be considered at all as a dielectric, and in fact the impedance behavior of the nanoporous electrode can be described as a transmission line equivalent circuit that extends over the whole porous structure.[19] The present study is restricted to those steady states where the TiO_2 porous network is basically an electrical insulator. An experimental study of the porous network impedance in accumulation conditions has been reported elsewhere.[20]

Models

Capacitance and potential distribution of a nanoporous electrode in the dielectric state.—In the nanoporous electrode the conducting substrate is in contact both with the electrolyte and the TiO_2 particles. These two pathways, shown in Fig. 1, provide different capacitive contributions. For path i, SnO_2(F)/electrolyte junction, the behavior of the capacitance and the potential distribution are discussed in Appendix A.

In the sintering process the nanoparticles stick to the substrate surface and cover a part of the surface; hence, the electrical pathway ii in Fig. 1 relates to the part of the substrate surface where the SnO_2(F)/TiO_2 junction replaces the substrate/electrolyte contact. From the point of view of the electrical response, in path ii the Helmholtz layer over the bare substrate is replaced by a combination of two capacitances: a dielectric medium (TiO_2) with capacitance/area C_d, and a Helmholtz layer at the dielectric-electrolyte contact, having a capacitance/area gC_H. The factor g accounts for a possible increase of the area of the Helmholtz layer over the dielectric, with respect to the substrate area that is covered by the dielectric. Since it is assumed that the amount of dopant in the covering material is negligible, it is expected according to our previous study[2] that the region the field penetrates into the nanostructure is independent of the applied potential. This understanding justifies treating the porous semiconductor network as a constant capacitance, C_d. In addition, we expect[2] that the electrical field lines penetrate the nanoporous structure not much further than the first particle; hence, g should not be much larger than 1. This point is further considered later on.

The dielectric capacitance for TiO_2 can be estimated as

$$C_d = \frac{\varepsilon_{r2} \varepsilon_0}{t} \quad [2]$$

where $\varepsilon_{r2} \approx 50$ and t is the thickness of the dielectric layer, so that C_d ranges from 4 to 1 $\mu F/cm^2$ for $t = 10$-50 nm. Usually the Helmholtz capacitance is about $C_H = 10\ \mu F/cm^2$.

Hence, in path ii, the dielectric and the Helmholtz layer over the dielectric, considered jointly, constitute a constant capacitor with capacitance (per TiO_2 covered unit area of contact with the substrate)

$$C_{ns} = [1/C_d + 1/(gC_H)]^{-1} \quad [3]$$

Therefore, the analysis of Appendix A for the substrate/electrolyte junction (path i) can be repeated for path ii of Fig. 1. In this case Eq. A-10 gives

$$\frac{1}{C^2} = \frac{2}{N_D e \varepsilon_r \varepsilon_0}(V_a + U_0) + \left(\frac{1}{C_d} + \frac{1}{gC_H}\right)^2 \quad [4]$$

Combining the two branches i and ii, when a fraction f of the surface of the conducting film is covered by the dielectric medium, we find the expression of the total capacitance

$$C = (1 - f)C_i + fC_{ii} \quad [5]$$

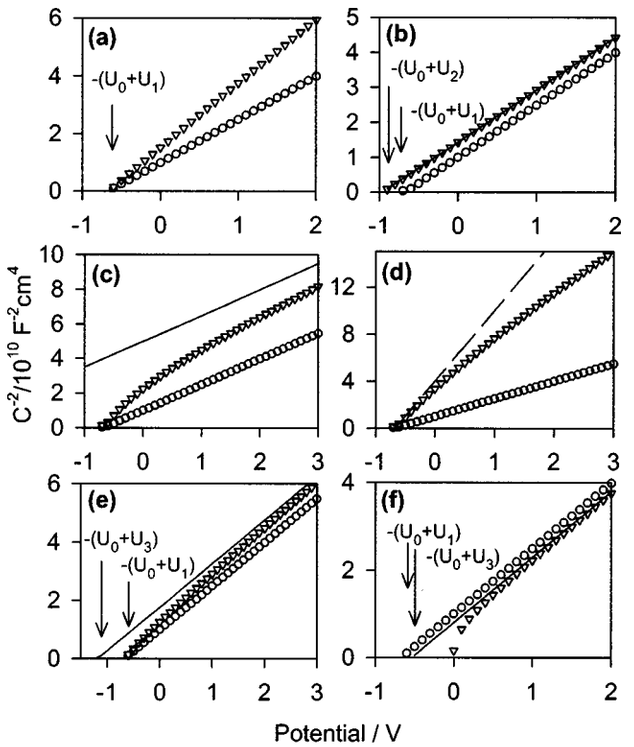

Figure 2. Simulations of the capacitance of bare and TiO_2 covered SnO_2(F) electrodes in contact with solution. (○) The bare SnO_2(F) substrate, with $N_D = 10^{21}$ cm^{-3}, $\varepsilon_r = 9$, $C_H = 10\,\mu$F cm^{-2}, and $U_0 = 0$ V. (▽) The electrode with a dielectric that covers totally or partially the substrate surface. (a) Covering by a TiO_2 nanoporous film, with a fraction $f = 0.2$ of the substrate covered from the electrolyte. The specific capacitance of the nanoparticles is very small, $C_d = 0.05C_H$, so that the part covered makes no contribution to the overall capacitance (see text). The apparent flatband potential $-(U_0 + U_1)$ is indicated. (b) Complete covering ($f = 1, g = 1$) with a thin dielectric layer with $C_d = 5C_H$. (c) Half covering ($f = 0.5, g = 1$) with dielectric capacitance $C_d = 0.5C_H$. (d) Half covering ($f = 0.5, g = 1$) with dielectric capacitance $C_d = 0.1C_H$. (— — —) The capacitance of the 50% free substrate area. (e) Covering by a TiO_2 nanoporous film, with a fraction $f = 0.2$ of the substrate covered from the electrolyte, area enhancement factor $g = 5$, and dielectric capacitance $C_d = 0.5C_H$. (f) Same as (e) with $g = 50$, $C_d = 10C_H$. (——) The asymptotic expression of the capacitance, Eq. 9.

A main purpose of this formula is to compare the capacitance of the nanoporous electrode to that of the bare substrate in order to obtain information about the real state of the triple junction, substrate/(film, electrolyte). Since there are different possible configurations, particles sizes, materials, etc., we examine in the following a number of cases and their manifestation in the MS plots.

The dielectric covering completely blocks part of the surface.—If the specific capacitance of the dielectric covering is very small, $C_d \ll C_H$, the C_{ii} can be neglected in Eq. 5. The capacitance is determined by the substrate area exposed to the electrolyte. The MS plot of the covered electrode is then described by

$$\frac{1}{C^2} = \frac{2}{(1-f)^2 N_D e \varepsilon_r \varepsilon_0}(V_a + U_0 + U_1) \qquad [6]$$

In this case the covered electrode shows the same apparent flatband as the bare electrode, $-(U_0 + U_1)$, but the covered electrode exhibits a larger slope, as shown in Fig. 2a. This case is quite interesting because it allows determination of the real fraction amount of free substrate area, $(1 - f)$, in a very simple way.

The dielectric layer covers the substrate completely.—Sometimes a thin dielectric layer is fabricated on the substrate prior to the deposition of the nanostructure in order to prevent the contact of the substrate with the electrolyte. Alternatively, an insulating polymer is grown in the bottom of these pores in order to block the pinholes. In connection with these manipulations, we now consider that the substrate has been covered completely with a dielectric layer of thickness *t*, *i.e.*, $f = 1$ and $g = 1$ in the notation introduced. This case is also relevant for organic layers deposited on semiconductor surfaces. The MS plot of the covered electrode follows Eq. 4, which can be expressed as

$$\frac{1}{C^2} = \frac{2}{N_D e \varepsilon_r \varepsilon_0}(V_a + U_0 + U_2) \qquad [7]$$

where

$$U_2 = \frac{N_D e \varepsilon_r \varepsilon_0}{2C_{ns}^2} = \frac{N_D e \varepsilon_r \varepsilon_0}{2}\left(\frac{1}{C_H} + \frac{1}{C_d}\right)^2 \qquad [8]$$

In this case the MS plot of the covered electrode is parallel to that of the bare substrate, as shown in Fig. 2b. The apparent flatband shifts negatively, with respect to the substrate, by $(U_2 - U_1)$.

With respect to full coverage of the substrate we briefly mention another possible behavior which was described elsewhere[21] for thick surface covering layer and non-negligible amount of dopant. In this case as the applied potential increases from $-U_0$, first an increasing depletion region is formed in the surface layer, and when the space-charge region reaches the whole thickness, *t*, the depletion layer continues to grow into the substrate. The consequence is a MS plot with two different consecutive slopes as shown in Ref. 21.

Partial covering of the substrate surface, with mixed contribution from free and covered surface.—If the dielectric capacitance C_d is not too small, then one must consider both contributions from paths i and ii using the general formula Eq. 5, where Eq. A-10 and 4 describe C_i and C_{ii}, respectively. The resulting expression cannot be written in a simple way, apart from the particular cases already examined in the two previous sections. We can, however, see that when the applied potential V_a is large (positive), the mixed capacitor in the surface is no longer important, because as the depletion capacitor C_b in Eq. A-1 decreases, the potential drop will be mainly into the substrate. Therefore the MS plots for bare substrate and covered electrode must be parallel at sufficiently positive potential. In fact it can be shown that Eq. 5 reduces, at large positive V_a, to

$$\frac{1}{C^2} = \frac{2}{N_D e \varepsilon_1}(V_a + U_0 + U_3) \qquad [9]$$

where

$$U_3 = \frac{N_D e \varepsilon_1}{2}\left[(1-f)\frac{1}{C_H^2} + f\left(\frac{1}{C_d} + \frac{1}{gC_H}\right)^2\right] \qquad [10]$$

In the particular case of $f = 1$, Eq. 9 reduces trivially to Eq. 7, which gives the case shown in Fig. 2b of parallel lines. However, for partial covering Eq. 9 is not a very strict criterion, because the potential required to make the surface capacitors unimportant may be impractically large. Consequently, in the practical range of measurement one may indeed observe different slopes. Nonetheless, Eq. 9 is useful in describing the trends of the data for a partially covered electrode, as illustrated in the following.

In Fig. 2c and d we show the simulations for 50% surface coverage. In Fig. 2c the dielectric capacitance $C_d = 0.5C_H$ is not negligible; hence, it may be appreciated that the capacitance line for the covered electrode tends to become parallel to that of the bare electrode. However, the behavior predicted by Eq. 9, shown by a continuous line in Fig. 2c, is not reached by the capacitance data in the

practical range. In Fig. 2d, the dielectric capacitance is small, $C_d = 0.1C_H$; thus, at the potentials close to the apparent flatband the free substrate surface determines the capacitance of the covered electrode, as shown by the dotted line, that corresponds to Eq. 6. Nonetheless, the dielectric covering exerts an increasing influence as the potential becomes more positive, giving rise to the downward curvature of the $1/C^2$ line.

The dielectric capacitance spreads through the nanoporous network.—So far it has been assumed that the dielectric contribution to the capacitance consists of a thin layer, or a set of single particles contacting the substrate; hence, in the previous analysis the area-enhancing factor was $g = 1$. Finally, we consider the possibility that the electrical field enters the nanostructure to a considerable extent, although emphasizing that this situation is unlikely because of the effective shielding by the liquid phase surrounding the nanoparticles. In Fig. 2e and f we take a low covering fraction $f = 0.2$, which is expected in a nanoporous electrode in which no intentional covering of the substrate was performed. In Fig. 2e the area-enhancing factor is $g = 5$, and the behavior of the capacitance due to this event is similar to that already commented in connection to Fig. 2c. In Fig. 2f we assume a large enhancement of $g = 50$ and a dielectric capacitance C_d which is larger than the Helmholtz capacitance. As a result the capacitance of the nanoporous electrode is larger than that of the bare electrode, so in this case the MS line of the covered electrode is below the substrate line.

Potential distribution.—Let us consider semiconductor nanoparticles attached to a conducting substrate as shown in Fig. 1. The total potential difference between the bulk of the substrate and the bulk of the solution, V_{tot}, is distributed differently in the two paths, i and ii, as indicated in Fig. 1. The potential distribution in path i is described in the Appendix. Let us consider path ii. We denote V_{ns} the potential drop from the junction SnO_2/TiO_2 to the bulk solution, so that $V_{tot} = V_b + V_{ns}$ and $V_{ns} = V_d + V_H$, where V_d is the potential drop in the TiO_2 nanoparticles (see Fig. 1). We adopt again the assumption that the contribution of the TiO_2 nanoparticles is a constant capacitance C_d (assuming that the TiO_2 is in the dielectric state), in which case the total differential capacitance comprising the nanoparticle and the Helmholtz layer is a constant, C_{ns}, given by Eq. 3. The space charge in the substrate, Q_b in Eq. A-4, equals $Q_{ns} = C_{ns}V_{ns}$. Hence, we get

$$V_{ns} = 2U_2\left[\left(1 + \frac{V_a + U_0}{U_2}\right)^{1/2} - 1\right] \qquad [11]$$

where U_2 is defined in Eq. 8. The result in Eq. 11 allows determination of the three potential drops (Helmholtz, dielectric, and band bending) in which V_{tot} is divided in path ii. This potential distribution is consistent with the analysis developed in Ref. 2 about the junction potential, with the different notation $b = 2eU_2/k_BT$ in Eq. 54 of Ref. 2. Equation 11 is even more general than the previous analysis because it accounts explicitly for the effect of the Helmholtz layer over the nanoparticles.

Experimental

The effect of the coverage was studied by impedance spectroscopy over two different SnO_2(F) substrates, labeled FTO1, with an approximate sheet resistance of 20 Ω/□, and FTO2, with a sheet resistance between 10 and 15 Ω/□. Two pieces of FTO1 were covered with TiO_2 colloids of different average diameter, prepared as reported in Ref. 22, conforming samples 100 and 102, and one piece of FTO2 was covered in a similar way with TiO_2 nanoparticles from Degussa P25 resulting on sample P25III. The characteristics of these samples are summarized in Table I.

Electrochemical measurements were done in a three-electrode cell using a platinum wire as counter electrode and a standard Ag/AgCl in 3 M KCl as reference electrode. The electrolytes used were solutions of distilled water adjusted to pH 11 and 2 with KOH and H_2SO_4, respectively. Impedance spectra were obtained with an Autolab PGSTAT-30 potentiostat equipped with an impedance analyzer and controlled by a PC.

Table I. Main characteristics of the samples used in this study.

Bare FTO		FTO covered with nanocrystalline TiO_2		
Sample name	Sheet resistance (Ω/□)	Sample name	Colloid diameter (nm)	Approx. composition
FTO1	20	100	91.1	100% anatase
		102	31.4	100% anatase
FTO2	10-15	P25111	25.0	70% anatase, 30% rutile

The range of potentials where these spectra were obtained was chosen to avoid both charge transfer from the SnO_2(F) to the electrolyte and electron accumulation in the TiO_2 nanoparticles. At these conditions the behavior of the samples was fully capacitive and, therefore, it was only necessary to consider the resistance of the electrolyte (in series) to obtain an equivalent circuit that describes well all the impedance spectra. The capacitance of the samples was obtained by fitting this simple RC series circuit to the measured impedance spectra. The calculated MS plots are shown in Fig. 3.

Results and Discussion

Figure 3a compares the capacitance results obtained for the bare FTO1 with those of samples 100 and 102 at pH 11, and Fig. 3b compares the capacitance of the bare FTO2 with that of sample P25III at two pH values. It can be seen that in the measurements corresponding to a given substrate and pH value, the two plots follow straight lines with the same apparent flatband potential but have

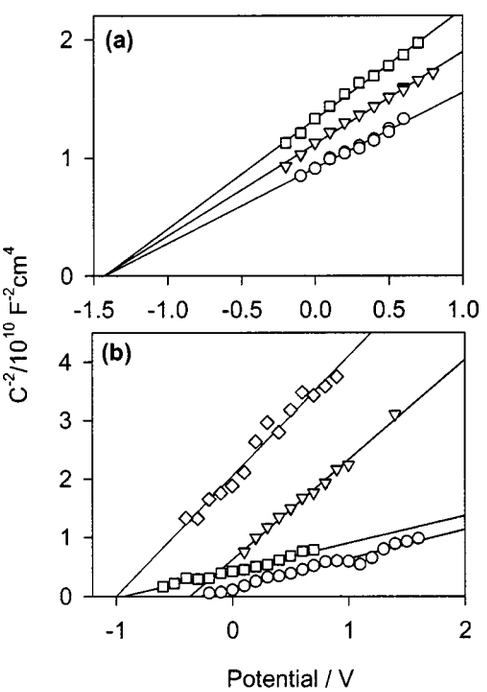

Figure 3. MS plots of the measured capacitance of the conducting substrates and the nanostructured TiO_2 electrodes listed in Table I. (a) Bare FTO1 and (○) nanoporous TiO_2 samples (□) 100 and (▽) 102 at pH 11. (b) Bare FTO2, at pH (○) 2 and (□) 11, and nanoporous TiO_2 sample P25III at pH (▽) 2 and (◇) 11.

different slopes, depending on the type of colloids deposited on the surface of the $SnO_2(F)$. This behavior is similar to the case described in the previous section in which the contribution to the capacitance due to the addition of the TiO_2 was considered negligible.

Therefore, for nanoporous TiO_2 electrodes the specific capacitance C_{ns} in Eq. 3 is much lower than C_H, which means that C_d and the factor g are small. This result supports the assumption that the field lines penetrate little into the TiO_2 network, not much further than the first particle, as suggested by several theoretical analyses.[2,4]

Because the deposition of the nanoparticles just reduces the effective substrate area that contributes to the capacity, that is $C = (1 - f)C_i$, it is possible to calculate the coverage factor, obtaining the values of 16% for sample 100, 10% for sample 102, and 70% for sample P25III. The difference of covering between the two first samples is related to the different average sizes of the colloids from which the films are made (see Table I).

The higher covering factor found for sample P25III is indicative of a greater affinity of the Degussa powder, which is a mixture of the crystalline structures anatase, 70%, and rutile, 30%, to stick over the $SnO_2(F)$ surface than that of samples 100 and 102 made from 100% anatase colloids. This fact may be explained on the basis of the lattice matching rules. As observed by X ray diffraction (XRD), the $SnO_2(F)$ surface is formed by cassiterite crystals with tetragonal unit cell with lattice parameters $a = 4.7$ and $c = 3.2$ Å. The structure of rutile TiO_2 phase contained in Degussa powder has the same unit cell and very similar lattice parameters, $a = 4.6$ and $c = 3.0$ Å, while the anatase unit cell is body centered tetragonal with parameters $a = 3.9$ and $c = 9.5$ Å, very different to those from the substrate. Therefore, it is easier for rutile to attach to and cover more fully the $SnO_2(F)$ surface than for anatase.

In Fig. 3b it is shown that changing the pH modifies the apparent flatband potential by 570 mV [for the measurements done on both the bare and covered $SnO_2(F)$], which is in good agreement with a 59 mV displacement per unit of pH. From the slopes of the MS plots of the two uncovered $SnO_2(F)$ samples, donor density was calculated, obtaining $N_D = 1.1 \times 10^{21}$ cm^{-3} for FTO1 and $N_D = 1.7 \times 10^{21}$ cm^{-3} for FTO2, which agrees with the lower sheet resistance of the second $SnO_2(F)$ sample. According to Eq. 1 this difference on the donor density (slope in the MS plot) is the cause of the different values of the apparent flatband potential at pH 11 that is observed in Fig. 3a and b. By using this difference and Eq. 1, the Helmholtz capacity was calculated to be $C_H = 9.3\ \mu$F cm^{-2} and thus, the flatband potential obtained is $-U_0 = -0.18$ V *vs.* Ag/AgCl (0.03 V *vs.* NHE).

Finally, we note that an earlier version of the model described has been used recently[23] to analyze the characteristics of the I_3^-/I^- redox couple in TiO_2-covered tin dioxide.

Conclusions

We have studied the capacitance characteristics of transparent conducting substrates such as SnO_2, totally or partially covered by a dielectric medium, in contact with an electrolyte. We showed that the triple contact, conducting substrate/(nanoporous film, electrolyte), can be studied by dark capacitance measurements, comparing the nanoporous film electrode with the bare substrate.

The theoretical analysis indicates two extreme cases. If the dielectric nanoparticles completely block part of the substrate surface, while the rest of the surface is exposed to the electrolyte, the increase of the MS slope is interpreted in terms of area reduction. The criterion for determining simply the fraction of surface coverage is to obtain linear MS plots with the same apparent flatband potential. The covering of a significant fraction of the surface by a thin dielectric layer shifts the apparent flatband negatively.

In the case of nanoporous TiO_2 electrodes, the capacitance contribution of the network in the dielectric state is very low, indicating that the field lines penetrate little into the TiO_2 network, not much further than the first particle. The different surface covering observed for rutile-anatase and pure anatase colloids is explained by lattice matching rules with the substrate.

The use of differently doped FTO substrates allowed the Helmholtz capacity to be calculated, and therefore, correction of the apparent flatband potential for the effect of band unpinning.

Acknowledgments

The authors acknowledge support of this work by la Comisión Interministerial de Ciencia y Tecnología under project PB98-1045. A.Z. is thankful for the support of the Israel Science Foundation founded by The Israel Academy of Science and Humanities.

Universitat Jaume I assisted in meeting the publication costs of this article.

Appendix: Mott-Schottky Plots of Degenerate Semiconductor Electrodes

The capacitance of the $SnO_2(F)$/electrolyte contact corresponds to path i in Fig. 1. The space-charge region at the SnO_2 surface provides a capacitance/area C_b (band bending)[16-18] which has the expression

$$C_b = \varepsilon_r \varepsilon_0 / w \qquad [A\text{-}1]$$

where ε_r is the dielectric constant of the SnO_2, ε_0 the permittivity of free space, and w is the width of the depletion region. If we denote N_D the dopant density, w can be expressed in terms of the band bending potential V_b and the positive elementary charge e, as

$$w = \left(\frac{2\varepsilon_r \varepsilon_0 V_b}{N_D e} \right)^{1/2} \qquad [A\text{-}2]$$

Let us denote $-U_0$ the electrical potential in the bulk of the SnO_2 film, with respect to a reference in solution, in equilibrium in the dark. As shown in Fig. 1, when a potential V_a is applied to the substrate, the total potential drop V_{tot} across the substrate/solution interface is

$$V_{tot} = U_0 + V_a \qquad [A\text{-}3]$$

The charge/area in the depletion layer is

$$Q_b = N_D w e \qquad [A\text{-}4]$$

In the Helmholtz layer it can be assumed that the differential capacitance C_H is a constant; hence, the integral capacitance equals the differential capacitance and the charge in the solution side of the surface is

$$Q_H = C_H V_H \qquad [A\text{-}5]$$

The charge-neutrality constraint $Q_b = Q_H$ can be written

$$V_1 V_b = V_H^2 \qquad [A\text{-}6]$$

where U_1 is defined in Eq. 1. Therefore

$$V_{tot} = V_b + V_H = V_b + (U_1 V_b)^{1/2} \qquad [A\text{-}7]$$

and solving these last two equations for V_H we get

$$V_H = 2U_1 \left[\left(1 + \frac{V_a + U_0}{U_1} \right)^{1/2} - 1 \right] \qquad [A\text{-}8]$$

The potential drop V_{tot} is shared by the two capacitors in series, C_b, and the Helmholtz capacitance/area C_H, hence

$$\frac{1}{C} = \frac{1}{C_b} + \frac{1}{C_H} \qquad [A\text{-}9]$$

Using these expressions for C_b and V_b, Eq. A-9 can be expressed in the form

$$\frac{1}{C^2} = \frac{2}{N_D e \varepsilon_r \varepsilon_0}(V_a + U_0) + \frac{1}{C_H^2} \qquad [A\text{-}10]$$

Thus, the apparent flatband potential determined from the MS plot is $-(U_0 + U_1)$.[15,18]

References

1. B. O'Regan and M. Grätzel, *Nature (London)*, **353**, 737 (1991).
2. J. Bisquert, G. Garcia-Belmonte, and F. Fabregat Santiago, *J. Solid State Electrochem.*, **3**, 337 (1999).
3. B. Levy, W. Liu, and S. E. Gilbert, *J. Phys. Chem. B*, **101**, 1810 (1997).
4. A. Zaban, A. Meier, and B. A. Gregg, *J. Phys. Chem. B*, **101**, 7985 (1997).
5. A. Shiga, A. Tsujiko, T. Ide, S. Yae, and Y. Nakato, *J. Phys. Chem.*, **102**, 6049 (1998).
6. K. Schwarzburg and F. Willig, *J. Phys. Chem. B*, **28**, 5743 (1999).
7. F. Pichot and B. A. Gregg, *J. Phys. Chem. B*, **104**, 6 (2000).
8. D. Cahen, G. Hodes, M. Grätzel, J. F. Guillemoles, and I. Riess, *J. Phys. Chem. B*, **104**, 2053 (2000).
9. J. van de Lagemaat, N.-G. Park, and A. J. Frank, *J. Phys. Chem. B*, **104**, 2044 (2000).
10. J. Ferber and J. Luther, *J. Phys. Chem. B*, **105**, 4895 (2001).
11. M. Turrión, B. Macht, H. Tributsch, and P. Salvador, *J. Phys. Chem. B*, **105**, 9732 (2001).
12. H. Tributsch, *Appl. Phys. A: Mater. Sci. Process.*, **73**, 305 (2001).
13. A. Solbrand, H. Lindström, H. Rensmo, A. Hagfeldt, S. E. Lindquist, and S. Södergren, *J. Phys. Chem. B*, **101**, 2514 (1997).
14. N. W. Duffy, L. M. Peter, R. M. G. Rajapakse, and K. G. U. Wijayantha, *Electrochem. Commun.*, **2**, 658 (2000).
15. R. de Gryse, W. P. Gomes, F. Cardon, and J. Vennik, *J. Electrochem. Soc.*, **125**, 711 (1975).
16. B. Pettinger, H.-R. Schöppel, T. Yokoyama, and H. Gerischer, *Ber. Bunsenges. Phys. Chem.*, **78**, 1024 (1974).
17. N. R. Armstrong, A. W. C. Lin, M. Fujihira, and T. Kuwana, *Anal. Chem.*, **48**, 741 (1976).
18. J. E. A. M. van den Meerakker, E. A. Meulenkamp, and M. Scholten, *J. Appl. Phys.*, **74**, 3282 (1993).
19. J. Bisquert, G. Garcia-Belmonte, F. Fabregat-Santiago, N. S. Ferriols, P. Bogdanoff, and E. C. Pereira, *J. Phys. Chem. B*, **104**, 2287 (2000).
20. F. Fabregat-Santiago, G. Garcia-Belmonte, J. Bisquert, A. Zaban, and P. Salvador, *J. Phys. Chem. B*, **106**, 334 (2002).
21. R. van de Krol, A. Gossens, and J. Schoonman, *J. Electrochem. Soc.*, **144**, 1723 (1997).
22. A. Zaban, S. T. Aruna, S. Tirosh, B. A. Gregg, and Y. Mastai, *J. Phys. Chem. B*, **104**, 4130 (2000).
23. L. M. Peter, N. W. Duffy, R. L. Wang, and K. G. U. Wijayantha, *J. Electroanal. Chem.*, **524-525**, 127 (2002).